Radiotherapy and Oncology 196 (2024) 110238

Contents lists available at ScienceDirect

Radiotherapy and Oncology

journal homepage: www.thegreenjournal.com

Original article

Infrared microspectroscopy to elucidate the underlying biomolecular mechanisms of FLASH radiotherapy☆

Immaculada Martínez-Rovira [a,*], Pierre Montay-Gruel [b,c], Benoît Petit [d], Ron J. Leavitt [d], Roberto González-Vegas [a], Pascal Froidevaux [e], Marjorie Juchaux [f], Yolanda Prezado [f], Ibraheem Yousef [g,1], Marie-Catherine Vozenin [d,h,1]

[a] Physics Department, Universitat Autònoma de Barcelona, 08193, Cerdanyola del Vallès (Barcelona), Spain
[b] Department of Radiation Oncology, Iridium Network, 2610, Wilrijk (Antwerp), Belgium
[c] Centre for Oncological Research (CORE), University of Antwerp, 2610, Antwerp, Belgium
[d] Laboratory of Radiation Oncology, Radiation Oncology Service and Oncology Department, Lausanne University Hospital and University of Lausanne, 1066, Lausanne, Switzerland
[e] Institute of Radiation Physics, Lausanne University Hospital and University of Lausanne, 1066, Lausanne, Switzerland
[f] Centre de recherche d'Orsay, Institut Curie, 91401, Orsay, France
[g] MIRAS Beamline, ALBA Synchotron, 08290, Cerdanyola del Vallès (Barcelona), Spain
[h] Radiotherapy and Radiobiology sector, Radiation Therapy service, University hospital of Geneva (Current address), 1205, Geneva, Switzerland

ARTICLE INFO

Keywords:
FLASH radiotherapy
Radiobiological studies
Infrared microspectroscopy

ABSTRACT

Background: FLASH-radiotherapy (FLASH-RT) is an emerging modality that uses ultra-high dose rates of radiation to enable curative doses to the tumor while preserving normal tissue. The biological studies showed the potential of FLASH-RT to revolutionize radiotherapy cancer treatments. However, the complex biological basis of FLASH-RT is not fully known yet.

Aim: Within this context, our aim is to get deeper insights into the biomolecular mechanisms underlying FLASH-RT through Fourier Transform Infrared Microspectroscopy (FTIRM).

Methods: C57Bl/6J female mice were whole brain irradiated at 10 Gy with the eRT6-Oriatron system. 10 Gy FLASH-RT was delivered in 1 pulse of 1.8 μs and conventional irradiations at 0.1 Gy/s. Brains were sampled and prepared for analysis 24 h post-RT. FTIRM was performed at the MIRAS beamline of ALBA Synchrotron. Infrared raster scanning maps of the whole mice brain sections were collected for each sample condition. Hyperspectral imaging and Principal Component Analysis (PCA) were performed in several regions of the brain.

Results: PCA results evidenced a clear separation between conventional and FLASH irradiations in the 1800–950 cm^{-1} region, with a significant overlap between FLASH and Control groups. An analysis of the loading plots revealed that most of the variance accounting for the separation between groups was associated to modifications in the protein backbone (Amide I). This protein degradation and/or conformational rearrangement was concomitant with nucleic acid fragmentation/condensation. Cluster separation between FLASH and conventional groups was also present in the 3000–2800 cm^{-1} region, being correlated with changes in the methylene and methyl group concentrations and in the lipid chain length. Specific vibrational features were detected as a function of the brain region.

Conclusion: This work provided new insights into the biomolecular effects involved in FLASH-RT through FTIRM. Our results showed that beyond nucleic acid investigations, one should take into account other dose-rate responsive molecules such as proteins, as they might be key to understand FLASH effect.

☆ This study was supported by the Spanish Ministry of Science, Innovation and Universities (grants RYC2018-024043-I and PID2020-114079RA-I00 to IMR), by the Spanish Association Against Cancer (grant IDEAS21849MART to IMR), by the Catalan Agency for Management of University and Research Grants (grant 2021 SGR 00607), and by the Swiss National Science Foundation grant MAGIC - FNS CRS II5_186369 (to MCV).

* Correspondence to: Physics Department, Universitat Autònoma de Barcelona, Campus UAB Bellaterra, Edifici C, Cerdanyola del Vallès (Barcelona), Spain.
E-mail address: Immaculada.martinez@uab.cat (I. Martínez-Rovira).

[1] I.Y. and M.-C.V contributed equally to this work.

https://doi.org/10.1016/j.radonc.2024.110238
Received 9 November 2023; Received in revised form 18 March 2024; Accepted 19 March 2024
Available online 26 March 2024

Introduction

FLASH-radiotherapy (FLASH-RT) is an emerging modality that uses ultra-high dose rates (>40 Gy/s), which are several orders of magnitude higher than the ones used in standard RT. This unexpected dose-rate effect was already reported in the 60–70s [1], but then abandoned. FLASH-RT in its present form was rediscovered in 2014 by Favaudon and collaborators [2] and reproduced in many laboratories over the world.

Today, a significant number of robust biological studies have proved the decrease in normal tissue toxicities and the efficacious anti-tumor response of FLASH-RT in multiple animal models using different beam types (photons, electrons, protons and carbon); see [3–6], among others. Preclinical data supporting FLASH-RT is continuously growing. Recently, the first clinical trial undergoing palliative FLASH-RT to extremity bone metastases has also been published [7].

The impressive results obtained in these biological studies opened the way for FLASH-RT to revolutionize RT cancer treatments. However, besides the physics and technological challenges, the complex biological basis of FLASH-RT is not fully known and there is an urgent need to understand the underlying biological mechanisms involved in these novel approaches to progress on the development of FLASH-RT.

It is clear that the involved mechanisms in FLASH-RT differ from the ones of conventional dose rates, and that they likely involve a combination of different biological, chemical and physical processes [6]. Mechanisms such as reduced DNA damage [8,9], reduced radiation-induced apoptosis [2], along with vascular, immune and inflammatory processes are being investigated [2,5,10,11]. Early hypotheses on the protective benefits of FLASH-RT have been associated to reactive oxygen species (ROS) recombination and diffusion [11–13]. More recently, the inverse effect between high dose rates and lipid peroxidation was considered as one plausible mechanism to explain the FLASH effect [14]. However, the full picture of the mechanisms underpinning the FLASH effect still needs to be uncovered.

Within this context, our objective is to shed some light on the FLASH-RT mechanisms by explaining *in situ* molecular alterations through Fourier Transform Infrared Microspectroscopy (FTIRM). FTIRM is a powerful analytical tool that allows to study the biomolecular characteristics of biological specimens. The composition, molecular structure or chemical modifications of the main biomolecules (including proteins, lipids, carbohydrates and nucleic acids) can be investigated [15]. The analysis of the biological components in tissues through FTIRM allowed to identify different disease states, to discriminate between diseased and healthy tissues, as well as to monitor tissue responses to different treatments, a few of them including RT [16–19].

The current study explores, for the first time, the capabilities of FTIRM to investigate the FLASH effect. In particular, we applied FTIRM imaging and principal component analysis (PCA) to monitor the molecular changes induced by FLASH-RT in mice brains at 24 h post-RT.

Materials and methods

Animals

All animal procedures were conducted in accordance with the Swiss ethics committee (VD3603) for animal experimentation. 10 weeks old female C57Bl/6J mice (purchased from Charles River Laboratories, France) were divided into two controls (labeled as Ctrl_1 and Ctrl_2), two animals irradiated with conventional dose rates (Conv_1 and Conv_2) and two animals irradiated with FLASH-RT (FLASH_1 and FLASH_2) ($n = 6$).

This exploratory study includes the biochemical imaging of the whole brain sections for each animal, which takes around 12 h measurement each. Considering such a long measurement time, the whole brain chemical mapping of a very large number of animals is not feasible. Moreover, it is important to keep in mind that conducting analyses on a limited number of animals becomes conventional when employing comprehensive omics methodologies. Despite the smaller sample size, these advanced techniques offer a wealth of information that is highly pertinent for gaining insights into complex biological processes. Additionally, it is important to acknowledge the use of rodents in these studies, as they provide a genetically and phenotypically homogeneous model, enhancing the reproducibility and reliability of the findings.

FLASH irradiations

Whole brain irradiations at 10 Gy were performed on a prototype Oriatron 6e (PMB Alcen, France), a 6-MeV electron beam linear accelerator (LINAC). Irradiations were done at the Lausanne University Hospital (Lausanne, Switzerland) as reported elsewhere [20]. FLASH-RT was delivered in 1 pulse of 1.8 μs and conventional irradiations at 0.1 Gy/s. Dosimetry has been extensively described and published to ensure reproducible reliable delivery [21–24].

Sample preparation

At 24 h post-RT, the whole brain was snap-frozen in isopentane cooled in liquid nitrogen. Prior to the FTIRM measurements, 4 μm-thick brain cryosections were deposited onto low-e microscope slides (Kevley Technologies). Sections were immersed in zinc formalin solution (Sigma-Aldrich) and then, rinsed with Millipore ultrapure water and dried.

FTIRM measurements and data analysis

FTIRM was performed at the MIRAS beamline of ALBA Synchrotron using the BRUKER 3000 Hyperion microscope coupled to a Vertex 70 spectrometer. For the measurements, a conventional infrared source was employed. Raster scanning maps (100×100 μm^2 spacing) of the whole mice brain section were collected for each sample condition. Each infrared spectrum was acquired in the mid-infrared range after 4 co-added scans with a 4 cm^{-1} spectral resolution, using a 15× Schwarzschild objective (NA = 0.4) and a liquid nitrogen-cooled mercury cadmium telluride (MCT) detector. The total acquisition time for each image was around 12 h, including the time for alignment and imaging.

Multivariate analysis was performed using the Quasar software [25]. PCA was performed on unit vector normalized second derivative spectra (Savitzky–Golay algorithm; 5 points filter; 3rd polynomial order). Second order derivation of the spectra allowed to enhance the discriminative features [26]. Two spectral regions were studied:

- 1800–950 cm^{-1}, with contributions from carbohydrates and phosphates associated with nucleic acids (DNA, RNA) in the low frequency range (1350–950 cm^{-1}). In the 1800–1400 cm^{-1} range, absorption is dominated by the peptide bonds of cell peptides and proteins.
- 3000–2800 cm^{-1}, mainly dominated by the symmetric and asymmetric stretching modes of methylene and methyl groups present in the hydrocarbon acyl chain length of lipids.

PCA was performed in different regions of interest (ROIs) of the brain sections:

- ROI 1: Hip SO (Hippocampus stratum oriens),
- ROI 2: Hip SP (Hippocampus pyramidal layer),
- ROI 3: Hip SR (Hippocampus stratum radiatum),
- ROI 4: Hip DG (Hippocampus dentate gyrus),
- ROI 5: Cortex FR/MO (Frontal and somatomor areas of the Cortex),
- ROI 6: Cb W (Cerebellum white matter),
- ROI 7: Cb G (Cerebellum gray matter).

Table 1
Main band assignments in the FTIRM spectra (ν = stretching vibration; s = symmetric; as = asymmetric).

Main band assignment	Spectral region (cm^{-1})	Reference
Phosphate III (PhIII)	984–950	[29]
Phosphate II (PhII)	1135–1004	[29]
Phosphate I (PhI)	1270–1186	[29]
Amide II (AII)	1585–1483	[30]
Amide I (AI)	1714–1585	[30]
$\nu_s CH_2$ (sCH_2)	2863–2838	[31]
$\nu_s CH_3$ (sCH_3)	2881–2865	[31]
$\nu_{as} CH_2$ ($asCH_2$)	2946–2900	[31]
$\nu_{as} CH_3$ ($asCH_3$)	2980–2946	[31]

In order to evaluate the area under the main spectral bands (see Table 1), a baseline correction method was applied to the spectral region under analysis (1800–950 cm^{-1} or 3000–2800 cm^{-1}). In particular, we assessed several integral ratios between these bands according to their biological significance. The relative protein secondary structure was also evaluated by calculating the area ratio of a range attributed to β-sheet (1640 cm^{-1}) and to one due to α-helix (1658 cm^{-1}) in the second derivatized spectra [27]. Since the assignment of the region around 1640 cm^{-1} could be equivocal [28], this band (labeled as βU) was associated to both β-sheet and to unordered structures. Hyperspectral imaging, as well as violin plots with the probability density of the data, were generated. Information on each specific ratio will be given along Section "Results and Discussion".

Statistical analyses were carried out using the software R. The non-parametric Kruskal–Wallis test was employed to assess significance between control and irradiated groups. Then, when global group effects were found to be statistically significant, a Dunn test for pairwise comparisons including the Bonferroni adjustment was performed.

Results and discussion

Section "Hyperspectral images" displays the images providing the biochemical architecture of brain sections under different irradiation conditions. Then, an analysis based on a multivariate approach is presented in Sections "PCA analysis in the 1800–950 cm^{-1} spectral region" and "PCA analysis in the 3000–2800 cm^{-1} spectral region". PCA results and the probability density of the data for several spectral ratios are presented. Discussion along the text will be focused on the regions presenting larger differences in the PCA (ROIs 4, 5 and 6) and on ROIs presenting different trends with respect to other regions (ROI 1). Data for ROIs 2, 3 and 7 is presented as supplementary information.

Hyperspectral images

Fig. 1 shows the hyperspectral images corresponding to the integration of several bands related to the major biomolecular components in biological samples: the Amide I (related to proteins), the Phosphate I and II (mostly related to nucleic acids), and the whole lipid region. One can clearly observe that distributions vary depending on the brain region, suggesting a variable sensitivity to dose rate-induced effects in the different brain regions. Therefore, a separated analysis for several regions within the cortex, the hippocampus (stratum oriens, pyramidal layer, and stratum radiatum) and the cerebellum (white matter and gray matter) was performed. Qualitatively, the chemical images highlight the similarity between FLASH and Ctrl groups and illustrate the differences between FLASH and Conv samples. Despite that the hyperspectral images provide a good overview on the biochemical modifications on the whole tissue structure, one should keep in mind that FTIRM generates very complex datasets and data analysis needs to be based on a multivariate approach, as presented in the next sections.

PCA analysis in the 1800–950 cm^{-1} spectral region

In this section, the main results for the 1800–950 cm^{-1} spectral region (mainly proteins, nucleic acids and carbohydrates) are summarized.

PCA was performed on the Savitzky–Golay second derivative data as an unsupervised method to identify the main sources of variation in the FTIRM spectra. Fig. 2 shows the PCA scores and the corresponding loadings, which indicate the influence of each wavenumber in the two main principal components PC1 and PC2. The PCA results are presented separately as a function of the ROI studied. Each ROI is composed by several pixels. In the PCA scores, each point represents the projection of the infrared spectrum corresponding to each one of these pixels. The different colors indicate the different irradiation modalities. The percentage of the total variance described by these two PCs is around 67%–75%, depending on the configuration, except in the case of ROI 1. In the later case, PC3 has been also included as a supplementary material.

In general, PCA scatter plots display well-separated clusters between Conv and FLASH irradiations, mostly separating along PC1. Most of the variance accounting for the separation of Conv groups is associated with conformational changes in the Amide I band, which is assigned to the C=O stretching vibrations, with some contributions from the out-of-phase CN stretching vibration, the CCN deformation and the NH in-plane bend [30]. There is some contribution from the Amide II band, related to the NH in-plane bend and the CN stretching vibration [30]. These modifications are related to changing protein morphologies.

A significant overlap between non-irradiated and FLASH configurations is observed in most ROIs, with some separation along PC2. The PC2 loading plots show most of the contributions from the Amide I and Amide II bands. In some ROIs (especially ROI 1, ROI 2, ROI 5 and ROI 7) there is a contribution from the infrared peak at 1467 cm^{-1}, associated to the symmetric bending of the methylene groups. The 1500–1300 cm^{-1} region includes complex absorptions from CH_2 and CH_3 bending modes of lipids, proteins, and base-sugar vibrations of nucleic acids. Complementary information can be obtained from the 3000–2800 cm^{-1} spectral region, where the other deformation modes of these groups are located. There is also some contribution from the ester carbonyl stretching mode located at 1760–1718 cm^{-1}, sensitive to the glycerol-acyl chain interface modifications of ester lipids.

The major differences between irradiation configurations are detected in the cortex region (ROI 5), as well as in several hippocampus regions (specially in ROI 4, with a similar trend for ROI 2 and ROI 3), two regions highly involved in brain functions and memory. In general, PC1 and PC2 loading plots in the different ROI are relatively close in shape, showing the similarity of the biochemical changes induced. The features of ROI 1 (Hip SO) differ from the other ROIs, as shown in the distinct averaged absorbance spectra (see supplementary data); the PCA scores in this region displays a higher level of overlapping between both irradiation configurations with respect to the other ROIs in (PC1–PC2). However, in the PC3–PC1 and PC3–PC2 score plots, clear differences between irradiation modalities are observed (see supplementary material). Based on a recent fine-detail spatial transcriptomics approach [32], we determined that ROIs 1–4 all have excitatory neurons, astrocytes, and microglia. One specific cell type that is enriched in ROI 1 is somatostatin-positive (Sst+) CA1 interneurons. Based on these data, we suggest that Sst+ inhibitory gabaergic interneurons might have distinct radiation-induced response.

FLASH-RT induces a difference in protein signature

The Amide I and Amide II bands cannot provide structure information on a single protein type in complex systems such as the brain. However, changes in these bands are correlated with protein secondary structure modifications, being amide II less affected by the side chain vibrations. Instead, the amide I band of polypeptides and proteins is typically used for secondary structure analysis since it strongly depends

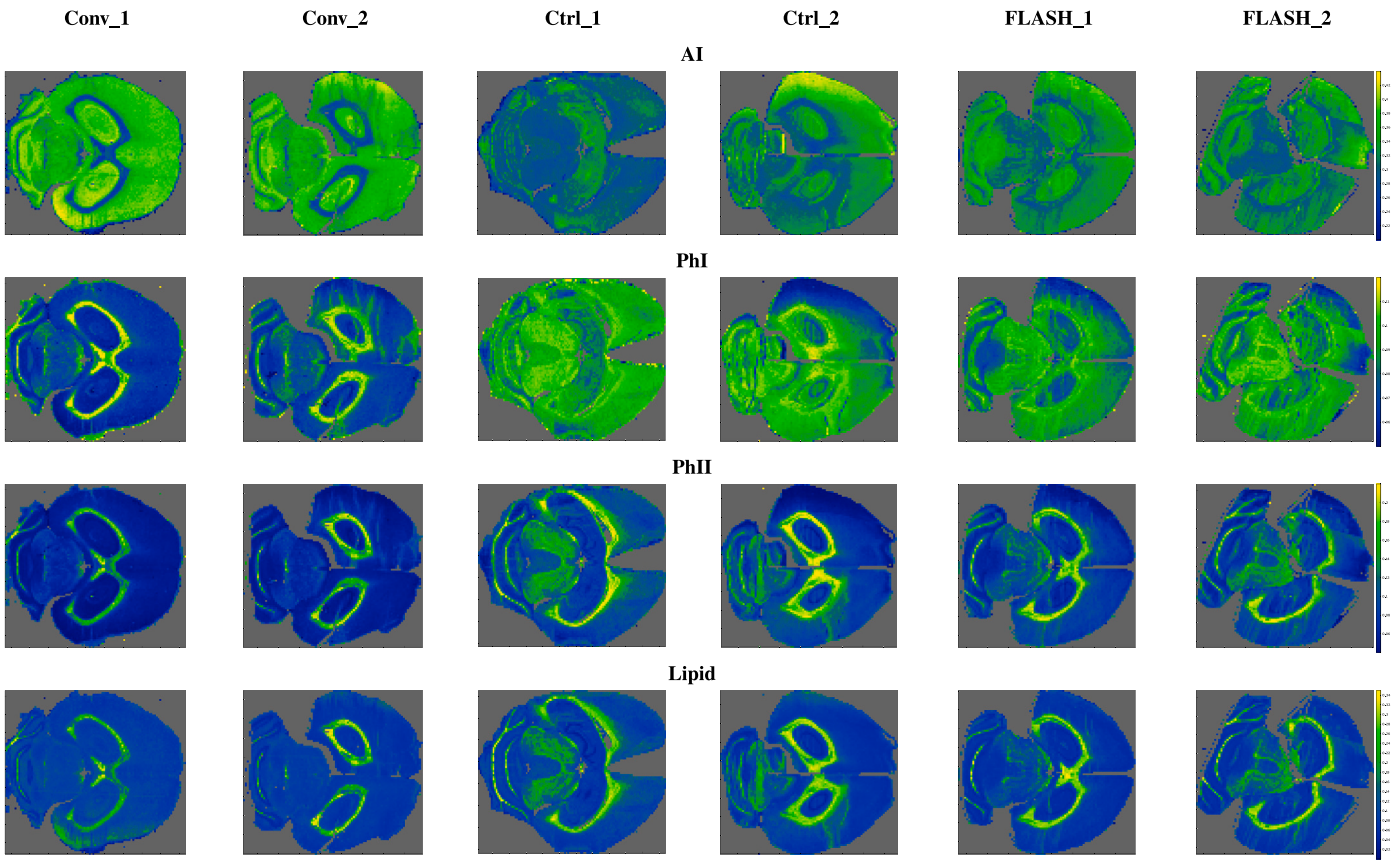

Fig. 1. Hyperspectral images of the AI, PhI, PhII spectral bands and the lipid region (3000–2800 cm^{-1}) for the different configurations (Controls: Ctrl_1 and Ctrl_2; Conventional irradiations: Conv_1 and Conv_2; FLASH irradiations: FLASH_1 and FLASH_2). Color bar (right): Blue color indicates regions with low values, while yellow color corresponds to high values. (For interpretation of the references to color in this figure legend, the reader is referred to the web version of this article.)

on the structure of the protein backbone. The Amide I region has also been extensively used to indicate the predominance of α-helical and β-sheet structures of proteins since each secondary structure absorbs in a specific range within the Amide I mode [30].

In order to elucidate changes in the protein structural components due to the two types of irradiations in comparison with control samples, the area ratio of the spectral range attributed to a β-sheet to the one due to an α-helix were statistically analyzed, as shown in Fig. 4 (top). Results show an increased number of cellular proteins having a β-sheet secondary structure with respect to α-helix for Conv samples, implying that protein conformations vary in relation to each other based on the type of irradiation. In ROIs 2 and 4, statistical differences between FLASH and Ctrl are not significant.

Structural changes in the cellular proteins were previously associated to a signature of cell death due to a different distribution of proteins during apoptosis or to denaturation of the existing proteins [33]. Also, protein peroxidation after irradiation leads to the formation of protein-carbonyl and, mostly, protein hydroperoxides, in addition to protein-gluthatinisation and Pr-S-S-Pr bridging in cystein-containing proteins. Thus protein peroxidation in Conv samples might induce a significant difference in infrared spectrum, particularly in the C=O absorption domain.

The PCA results and the integral band ratios indicate a clear heterogeneity in the protein secondary structures between irradiation modalities. Despite FLASH effects in proteins have not been extensively studied, these results could suggest that proteins constitute key targets in dose-rate-dependent radiation effects. A recent study also confirmed that peptides in solution are oxidatively modified as a function of the dose rate [34].

FLASH-RT induces reduced nucleic acid damage

Regarding nucleic acids, FTIRM possesses a high sensitivity for the detection of small conformational and structural modifications. Associated vibrations are detected in several regions within the 1800–950 cm^{-1} spectral range. In particular, in the range between 1270–1000 cm^{-1}, there are the strong absorptions of phosphate groups and of the sugar, and it contains bands sensitive to nucleic acid backbone conformation. It is important to mention that these bands could also contain contributions from head-group vibrations of phospholipids or phosphorylated species.

The second derivatized average spectra in this region is presented in the supplementary material, allowing the resolution of several characteristic subbands. Fig. 4 presents as well as the violin plots showing the distribution of the relative intensities of the PhI and PhII bands with respect to the proteins component (using the area of the Amide II), as performed in previous works [35,36].

In the PhI region, associated to the asymmetric phosphate stretching band of phosphodiester nucleic acids, we found the main markers for the A-form double-helix at 1240–1235 cm^{-1}, for the B-form at 1225–1220 cm^{-1} and for the Z helical form of DNA at 1216–1213 cm^{-1} [29,37], as well as other contributions. The second derivatized averaged spectra shows multiple changes in the absorbance within the PhI band, suggesting important changes in the nucleic acid structure and conformation as a function of the irradiation configuration, being FLASH irradiations closer to controls. Violin plots show a relative decrease of the PhI integral intensities for Conv irradiations with respect to Ctrl and FLASH groups for all ROIs (excepting ROI 1, that follows an inverse trend). FLASH configurations also present a small reduction of this band ratio with respect to Ctrl (statistical differences are not significant in ROI 4). This de-structuration of the PhI band was associated with the degradation of higher order DNA and to DNA condensation [35].

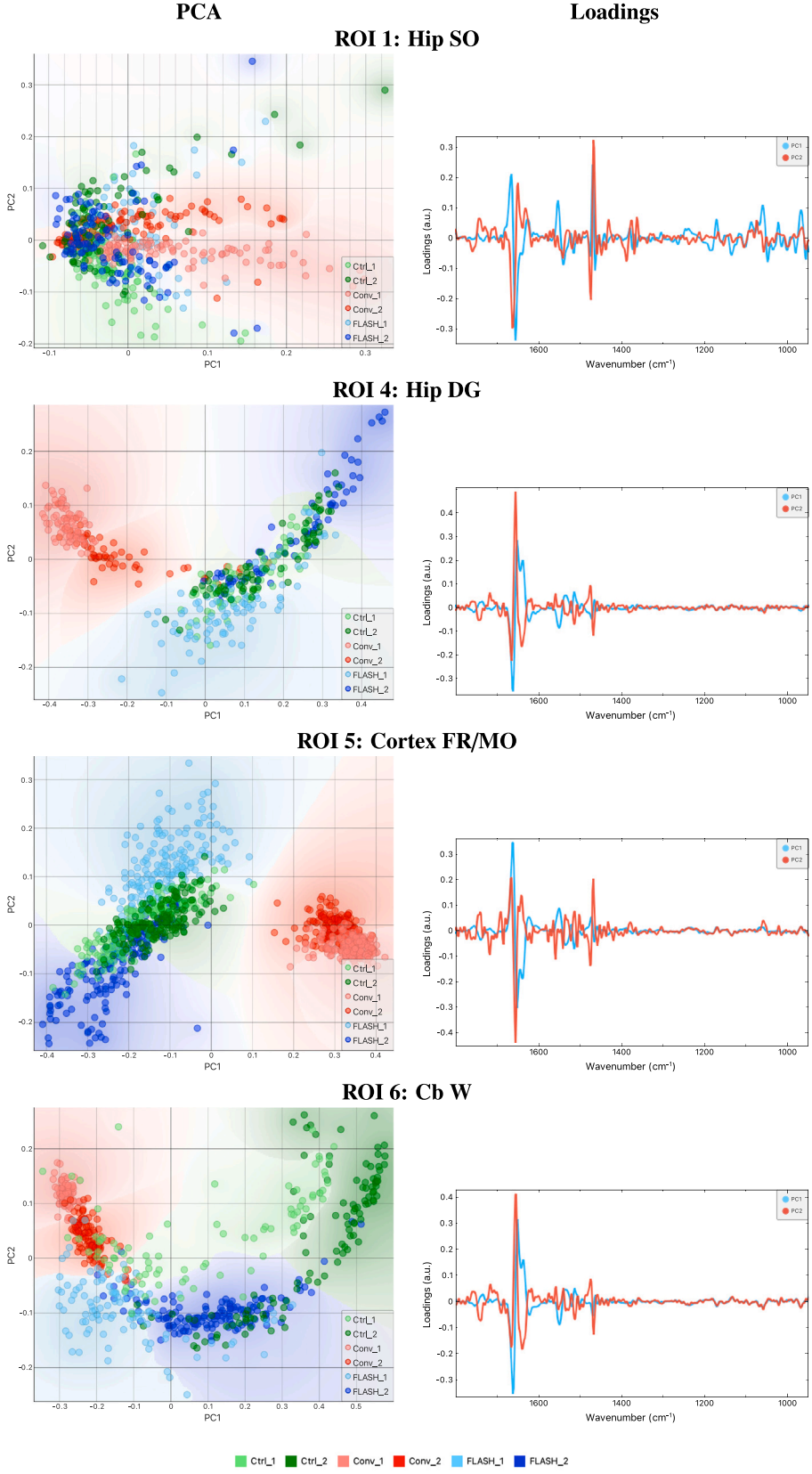

Fig. 2. 1800–950 cm^{-1} spectral region. PCA scores (PC1 *vs* PC2) and the corresponding loadings in ROIs 1, 4, 5 and 6. Each color in the PCA scores represents a specific configuration (Controls: Ctrl_1 and Ctrl_2; Conventional irradiations: Conv_1 and Conv_2; FLASH irradiations: FLASH_1 and FLASH_2). (For interpretation of the references to color in this figure legend, the reader is referred to the web version of this article.)

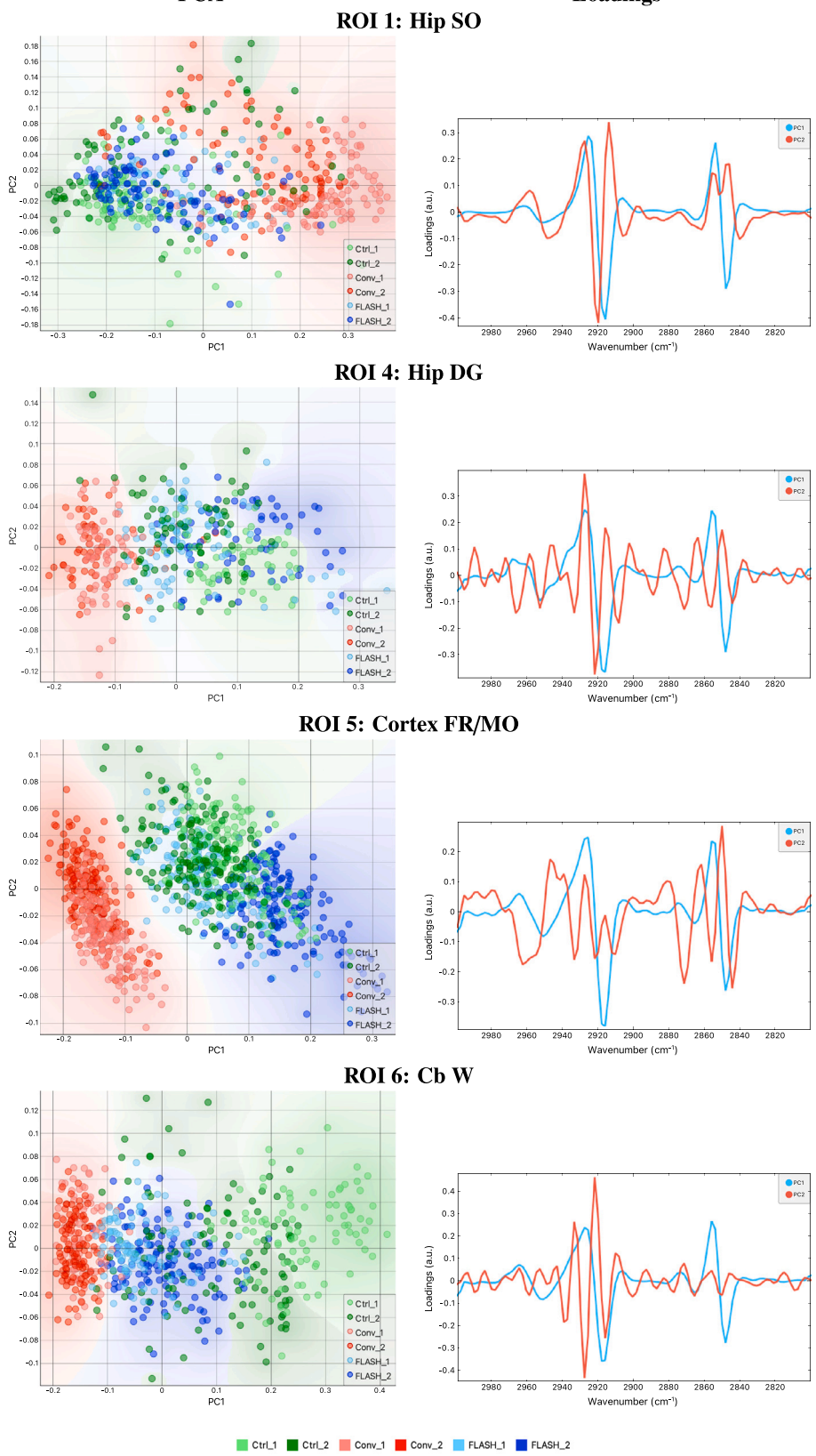

Fig. 3. 3000–2800 cm^{-1} spectral region. PCA scores (PC1 *vs* PC2) and the corresponding loadings in ROIs 1, 4, 5 and 6. Each color in the PCA scores represents a specific configuration (Controls: Ctrl_1 and Ctrl_2; Conventional irradiations: Conv_1 and Conv_2; FLASH irradiations: FLASH_1 and FLASH_2). (For interpretation of the references to color in this figure legend, the reader is referred to the web version of this article.)

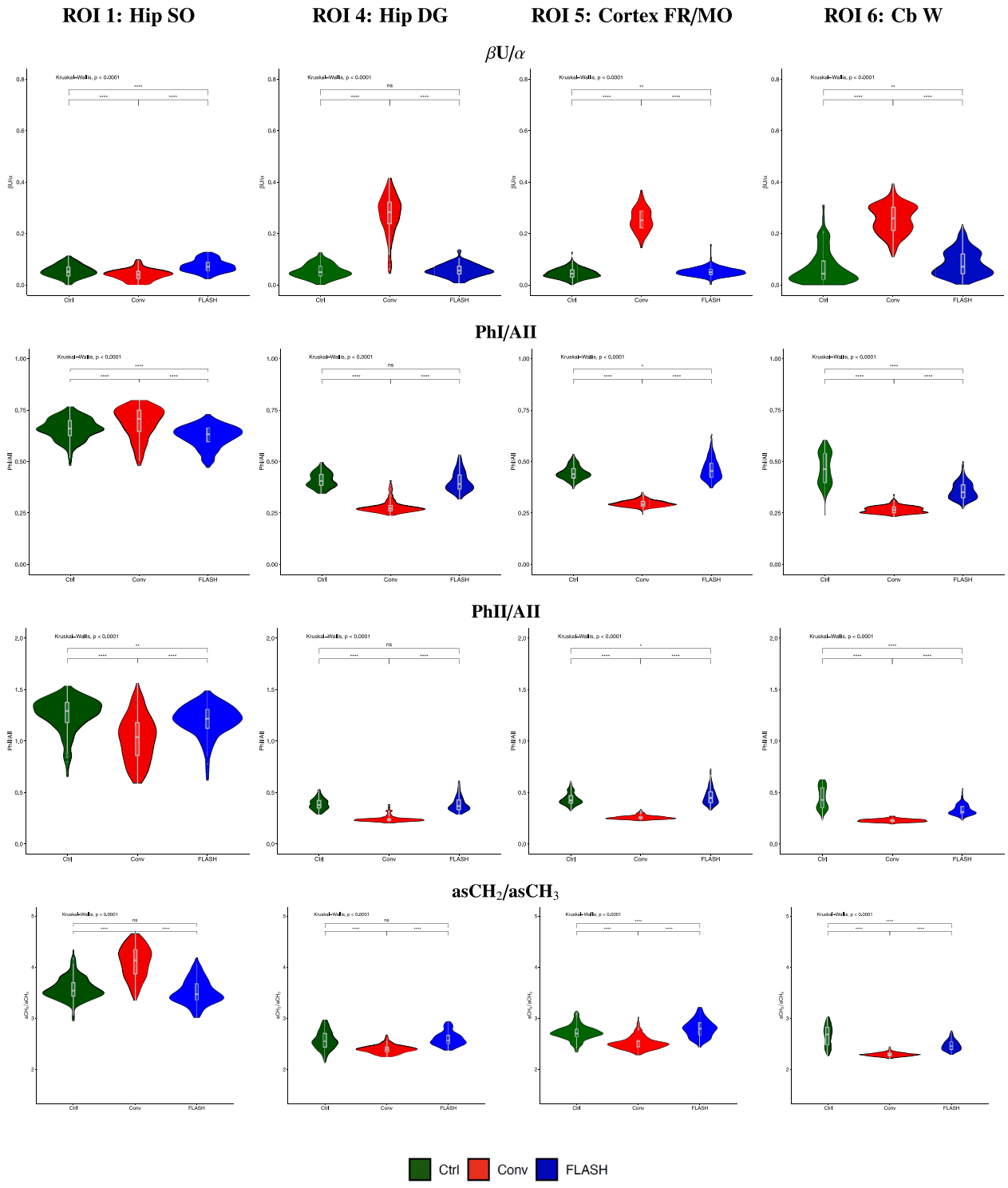

Fig. 4. Violin plots showing the distribution of the relative intensities of the $\beta U/\alpha$, PhI/AII, PhII/AII and $asCH_2/asCH_3$ spectral ratios (from top to bottom) in ROIs 1, 4, 5 and 6. The specific spectral ranges are reported in Table 1, which were determined based on the band intensities. *p*-value significance symbols are represented as follows: ns ($p > 0.05$), * ($p \leq 0.05$), ** ($p \leq 0.01$), *** ($p \leq 0.001$), **** ($p \leq 0.0001$). (For interpretation of the references to color in this figure legend, the reader is referred to the web version of this article.)

Spectroscopic evidence of such DNA damage under RT was previously reported [38].

The PhII band is composed by three major contributions, located at 1088 and 1060 and 1022 cm^{-1}, and other minor contributions. The first band is assigned to the symmetric PO_2^- stretching mode of nucleic acids (1088 cm^{-1}) and reflects the degree of intermolecular interactions in nucleic acids [16,29]. The other two bands are mostly associated to furanose vibrations (1060 and 1022 cm^{-1}) [29]; the furanose C–O stretching is a relevant marker for base pairing and base stacking in RNA [39]. The second derivative plot shows changes in several infrared bands within this range, indicating a distinct hydrogen bonding structures in the nucleic acids, as well as changes in the furanose and ribose structures. Similar to the PhI band, an important decrease in the relative intensity of the PhII band with respect to

the proteins component is observed for Conv irradiations. Previous works demonstrated that the PhII/AII ratio can be correlated with DNA fragmentation and cell death [35,40].

Between the PhI and PhII bands, one can also observe alterations of the carbohydrate metabolism, reflected also by the spectral shape modifications in the 1190–1140 cm^{-1} range.

In the low frequency range, intensity modifications in the PhIII band are indicative of ribose-phosphate main chain vibrations and follow the same trend as the PhI and PhII bands (data not shown). The decrease in absorbance of this band observed for Conv irradiations was previously attributed to backbone single and double strand breaks (SSD, DSB), crosslinks and sugar damage [38,39].

The role of DNA damage and repair in FLASH-RT is not completely clear. Our findings showing lower levels of nucleic acid at 24 h after FLASH *vs* Conv are consistent with previous reports in the normal lung [8] and blood cells [9]. However, a recent publication by Barghougth *et al.* using a DNA repair functional assay showed that FLASH does not affect chromosome translocations and junction structures more than Conv [41]. Further kinetic and functional studies will be required to elucidate the molecular mechanisms driven by FLASH-RT in the nucleic acids.

PCA analysis in the 3000–2800 cm^{-1} spectral region

In this section, the main results for the 3000–2800 cm^{-1} spectral region are reported. This region is mostly associated to the fatty acids of the various membrane amphiphiles (phospholipids). The vibrational modes in this region are known to be sensitive to lipid composition and membrane physical state. In particular, one can found the acyl chain vibrational modes related to carbon-hydrogen vibrations. The CH_2 asymmetric and symmetric stretching modes, along with the CH_3 asymmetric and symmetric stretching bands produce the highest absorbance values. The 3000–2800 cm^{-1} spectral region is specially relevant because it presents little overlap with other contributions and it is sensitive to conformational changes in the lipid acyl chain [31,42,43].

Fig. 3 displays the data distribution on the PC1/PC2 projection for the 3000–2800 cm^{-1} spectral range. In all cases, the first two principal components explain around 35%–60% of the total variance, except in the case of ROI 1 (89%). PCA delineates a clear separation between the FLASH-treated and the Conv-treated samples, mostly along PC1. As in the 1800–950 cm^{-1} spectral region, there is a significant overlap between spectra recorded under FLASH-RT conditions and controls. PC1 shows a correlation with the RT type (FLASH *versus* Conv), while PC2 describes the intra-group and inter-sample variability. The PC1 loading plots reveals that the Conv samples experience different molecular changes in the wave-numbers attributed to $asCH_2$ and sCH_2 stretching modes, and to the $asCH_3$ to a lesser extend. Changes in these bands are diagnostic of modifications in the hydrocarbon chain conformational order [44].

The largest cluster group separations in the PCA between irradiation configurations are detected in the cortex region (ROI 5), as well as in all the ROIs within the hippocampus. Loading plots in the different ROI are relatively similar in shape, showing a close correlation in the biochemical changes induced in these brain regions. The differences reported in this region seem to be less prominent than the ones reported in the 1800–950 cm^{-1} spectral region.

Fig. 4 (bottom part) presents the violin plots showing the distribution of the relative intensities of the $asCH_2/asCH_3$ ratio, associated to the chain length in lipids [43]. There is a general increase in the $asCH_3$ band with a concomitant decrease in the CH_2 bands for conventional irradiations in all ROIs (excepting ROI 1), implying a reduction of the $asCH_2/asCH_3$ band ratio for Conv irradiations with respect to FLASH and Ctrl. Statistical differences between FLASH and Ctrl are not significant in ROIs 1, 2 and 4.

Lipid bands of the infrared spectrum contain key information on lipid composition and membrane behavior that could be relevant to explain the FLASH effect. As stated in the introduction, the inverse effect of high dose rates and lipid peroxidation was considered as one plausible mechanism to explain the FLASH effect. Recently, it has been shown that FLASH-RT does not induce lipid peroxidation in lipids micelles and liposomes [14]. Several authors attempted to correlate the modifications on the infrared lipid vibrational modes with lipid peroxidation. Within this context, lipid peroxidation was associated with an increased methyl (CH_3) concentration [45,46] and with the loss of unsaturated acids [47–49]. While the increase in the $asCH_3$ band is observable for most ROIs in the Conv configurations, the decrease in the C–H stretching bands of unsaturated acyl chains is not observed (data not shown). Some works have also found a correlation between lipid peroxidation and the area under the ester carbonyl stretching mode (1760–1718 cm^{-1}), with respect to the total lipid component [50,51]. However, in our work we could not find a clear correlation between modifications in the ester carbonyl stretching mode and the RT modality.

Conclusions

In this study, we used FTIRM to rebuild the action of FLASH-RT on normal brain. The results of this work support the potential of FTIRM for analyzing biological components undergoing FLASH-RT. The advantage of FTIRM is that it allows the simultaneous observation of subtle molecular modifications of several functional groups related to proteins, nucleic acids, carbohydrates and lipids.

Distinct molecular changes were detected in the biochemical makeup of FLASH and Conv irradiations and, interestingly, a significant overlap was observed between FLASH and Ctrl groups. Multivariate analysis in the 1800–950 cm^{-1} spectral region showed that one of the major modifications was related to the structure of the protein backbone (Amide I), revealing an increase in the β-sheet content with respect to the α-helical secondary structure in conventional RT. This protein conformational rearrangement was concomitant with nucleic acid fragmentation/condensation, as shown in the analysis of the PhI, PhII and PhIII bands. Protein oxidation could also bring significant modifications in the C=O stretching mode, possibly due to formation of protein-carbonyls. Differences in the methylene and methyl group concentrations and in the lipid chain length also indicated distinct lipid structural and biochemical perturbations in FLASH-RT with respect to conventional irradiations. Vibrational features were ROI-dependent.

This study provides a molecular screenshot at 24 h post-irradiation time. Results show that beyond nucleic acid investigations, one should take into account other dose-rate responsive molecules such as proteins, as they might be key to understand FLASH effect. However, one should keep in mind that monitoring the overall changes occurring in tissues upon FLASH irradiations is a very complex task and would require both kinetic and functional studies. In particular, further studies investigating the impact at later time points will help us to assess the functional significance of our findings.

CRediT authorship contribution statement

Immaculada Martínez-Rovira: Writing – original draft, Validation, Software, Methodology, Investigation, Funding acquisition, Formal analysis, Conceptualization. **Pierre Montay-Gruel:** Writing – review & editing, Methodology. **Benoît Petit:** Resources, Methodology, Investigation. **Ron J. Leavitt:** Writing – review & editing, Methodology. **Roberto González-Vegas:** Investigation. **Pascal Froidevaux:** Writing – review & editing, Methodology. **Marjorie Juchaux:** Methodology. **Yolanda Prezado:** Conceptualization. **Ibraheem Yousef:** Writing – review & editing, Validation, Methodology, Investigation, Funding acquisition, Conceptualization. **Marie-Catherine Vozenin:** Writing – review & editing, Validation, Methodology, Investigation, Funding acquisition, Conceptualization.

Declaration of competing interest

None

Data availability

Research data will be stored in the CORA research data repository and it will be shared upon request to the corresponding author.

Acknowledgments

This study was supported by the Spanish Ministry of Science, Innovation and Universities (RYC2018-024043-I, PID2020-114079RA-I00 to IMR), by the Spanish Association Against Cancer (IDEAS21849MART to IMR), by the Catalan Agency for Management of University and Research Grants (2021 SGR 00607) and by the Swiss National Science Foundation grant MAGIC - FNS CRS II5_186369 (to MCV). Infrared experiments were performed at MIRAS beamline at ALBA Synchrotron Light Source Facility with the collaboration of ALBA staff. The authors would like to thank Kevin Sprengers, Ryan Paisley and Veljko Grilj for support doing irradiations.

Supplementary data

Supplementary material related to this article can be found online at https://doi.org/10.1016/j.radonc.2024.110238.

References

[1] Hornsey S, Alper T. Unexpected dose-rate effect in the killing of mice by radiation. Nature 1966;210(5032):212–3. http://dx.doi.org/10.1038/210212a0.
[2] Favaudon V, Caplier L, Monceau V, Pouzoulet F, Sayarath M, Fouillade C, et al. Ultrahigh dose-rate FLASH irradiation increases the differential response between normal and tumor tissue in mice. Sci Transl Med 2014;6(245):245ra93. http://dx.doi.org/10.1126/scitranslmed.3008973.
[3] Hughes JR, Parsons JL. FLASH radiotherapy: Current knowledge and future insights using proton-beam therapy. Int J Mol Sci 2020;21(18). http://dx.doi.org/10.3390/ijms21186492.
[4] Gao Y, Liu R, Chang C-W, Charyyev S, Zhou J, Bradley JD, et al. A potential revolution in cancer treatment: A topical review of FLASH radiotherapy. J Appl Clin Med Phys 2022;23(10):e13790. http://dx.doi.org/10.1002/acm2.13790.
[5] Vozenin M-C, Bourhis J, Durante M. Towards clinical translation of FLASH radiotherapy. Nat Rev Clin Oncol 2022;19(12):791–803. http://dx.doi.org/10.1038/s41571-022-00697-z.
[6] Limoli CL, Vozenin M-C. Reinventing radiobiology in the light of FLASH radiotherapy. Annu Rev Cancer Biol 2023 2023;7:1–21.
[7] Mascia AE, Daugherty EC, Zhang Y, Lee E, Xiao Z, Sertorio M, et al. Proton FLASH radiotherapy for the treatment of symptomatic bone metastases: The FAST-01 nonrandomized trial. JAMA Oncol 2023;9(1):62–9. http://dx.doi.org/10.1001/jamaoncol.2022.5843.
[8] Fouillade C, Curras-Alonso S, Giuranno L, Quelennec E, Heinrich S, Bonnet-Boissinot S, et al. FLASH irradiation spares lung progenitor cells and limits the incidence of radio-induced senescence. Clin Cancer Res 2020;26(6):1497–506. http://dx.doi.org/10.1158/1078-0432.CCR-19-1440.
[9] Cooper CR, Jones D, Jones GD, Petersson K. FLASH irradiation induces lower levels of DNA damage ex vivo, an effect modulated by Oxygen tension, dose, and dose rate. Br J Radiol 2022;95(1133):20211150. http://dx.doi.org/10.1259/bjr.20211150.
[10] Simmons DA, Lartey FM, Schüler E, Rafat M, King G, Kim A, et al. Reduced cognitive deficits after FLASH irradiation of whole mouse brain are associated with less hippocampal dendritic spine loss and neuroinflammation. Radiother Oncol 2019;139:4–10. http://dx.doi.org/10.1016/j.radonc.2019.06.006.
[11] Montay-Gruel P, Acharya MM, Petersson K, Alikhani L, Yakkala C, Allen BD, et al. Long-term neurocognitive benefits of FLASH radiotherapy driven by reduced reactive oxygen species. Proc Natl Acad Sci U S A 2019;116(22):10943–51. http://dx.doi.org/10.1073/pnas.1901777116.
[12] Spitz DR, Buettner GR, Petronek MS, St-Aubin JJ, Flynn RT, Waldron TJ, et al. An integrated physico-chemical approach for explaining the differential impact of FLASH versus conventional dose rate irradiation on cancer and normal tissue responses. Radiother Oncol 2019;139:23–7. http://dx.doi.org/10.1016/j.radonc.2019.03.028.
[13] Labarbe R, Hotoiu L, Barbier J, Favaudon V. A physicochemical model of reaction kinetics supports peroxyl radical recombination as the main determinant of the FLASH effect. Radiother Oncol 2020;153:303–10. http://dx.doi.org/10.1016/j.radonc.2020.06.001.
[14] Froidevaux P, Grilj V, Bailat C, Geyer WR, Bochud F, Vozenin M-C. FLASH irradiation does not induce lipid peroxidation in lipids micelles and liposomes. Radiat Phys Chem 2023;205:110733. http://dx.doi.org/10.1016/j.radphyschem.2022.110733.
[15] Baker MJ, Trevisan J, Bassan P, Bhargava R, Butler HJ, Dorling KM, et al. Using Fourier transform IR spectroscopy to analyze biological materials. Nat Protoc 2014;9(8):1771–91. http://dx.doi.org/10.1038/nprot.2014.110.
[16] Gault N, Lefaix J-L. Infrared microspectroscopic characteristics of radiation-induced apoptosis in human lymphocytes. Radiat Res 2003;160(2):238–50. http://dx.doi.org/10.1667/rr3020.1.
[17] Lipiec E, Bambery KR, Heraud P, Hirschmugl C, Lekki J, Kwiatek WM, et al. Synchrotron FTIR shows evidence of DNA damage and lipid accumulation in prostate adenocarcinoma PC-3 cells following proton irradiation. J Mol Struct 2014;1073:134–41. http://dx.doi.org/10.1016/j.molstruc.2014.04.056, Molecular Spectroscopy – An Interdisciplinary Approach.
[18] Yousef I, Seksek O, Gil S, Prezado Y, Sulé-Suso J, Martínez-Rovira I. Study of the biochemical effects induced by X-ray irradiations in combination with gadolinium nanoparticles in F98 glioma cells: first FTIR studies at the Emira laboratory of the SESAME synchrotron. Analyst 2016;141(7):2238–49. http://dx.doi.org/10.1039/c5an02378e.
[19] Martínez-Rovira I, Seksek O, Yousef I. A synchrotron-based infrared microspectroscopy study on the cellular response induced by gold nanoparticles combined with X-ray irradiations on F98 and U87-MG glioma cell lines. Analyst 2019;144:6352–64. http://dx.doi.org/10.1039/C9AN01109A.
[20] Jaccard M, Durán MT, Petersson K, Germond J-F, Liger P, Vozenin M-C, et al. High dose-per-pulse electron beam dosimetry: Commissioning of the oriatron eRT6 prototype linear accelerator for preclinical use. Med Phys 2018;45(2):863–74. http://dx.doi.org/10.1002/mp.12713.
[21] Jaccard M, Petersson K, Buchillier T, Germond J-F, Durán MT, Vozenin M-C, et al. High dose-per-pulse electron beam dosimetry: Usability and dose-rate independence of EBT3 Gafchromic films. Med Phys 2017;44(2):725–35. http://dx.doi.org/10.1002/mp.12066.
[22] Petersson K, Jaccard M, Germond J-F, Buchillier T, Bochud F, Bourhis J, et al. High dose-per-pulse electron beam dosimetry - A model to correct for the ion recombination in the Advanced Markus ionization chamber. Med Phys 2017;44(3):1157–67. http://dx.doi.org/10.1002/mp.12111.
[23] Jorge PG, Jaccard M, Petersson K, Gondré M, Durán MT, Desorgher L, et al. Dosimetric and preparation procedures for irradiating biological models with pulsed electron beam at ultra-high dose-rate. Radiother Oncol 2019;139:34–9. http://dx.doi.org/10.1016/j.radonc.2019.05.004.
[24] Montay-Gruel P, Petersson K, Jaccard M, Boivin G, Germond J-F, Petit B, et al. Irradiation in a flash: Unique sparing of memory in mice after whole brain irradiation with dose rates above 100Gy/s. Radiother Oncol 2017;124(3):365–9. http://dx.doi.org/10.1016/j.radonc.2017.05.003.
[25] Toplak M, Read ST, Sandt C, Borondics F. Quasar: Easy machine learning for biospectroscopy. Cells 2021;10(9). http://dx.doi.org/10.3390/cells10092300.
[26] Martínez-Rovira I, Seksek O, Puxeu J, Gómez J, Kreuzer M, Dučić T, et al. Synchrotron-based infrared microspectroscopy study on the radiosensitization effects of Gd nanoparticles at megavoltage radiation energies. Analyst 2019;144:5511–20. http://dx.doi.org/10.1039/C9AN00792J.
[27] André W, Sandt C, Dumas P, Djian P, Hoffner G. Structure of inclusions of Huntington's disease brain revealed by synchrotron infrared microspectroscopy: polymorphism and relevance to cytotoxicity. Anal Chem 2013;85(7):3765–73. http://dx.doi.org/10.1021/ac400038b.
[28] Ghimire H, Venkataramani M, Bian Z, Liu Y, Perera AGU. ATR-FTIR spectral discrimination between normal and tumorous mouse models of lymphoma and melanoma from serum samples. Sci Rep 2017;7(1):16993. http://dx.doi.org/10.1038/s41598-017-17027-4.
[29] Banyay M, Sarkar M, Gräslund A. A library of IR bands of nucleic acids in solution. Biophys Chem 2003;104(2):477–88. http://dx.doi.org/10.1016/S0301-4622(03)00035-8.
[30] Barth A. Infrared spectroscopy of proteins. Biochim Biophys Acta (BBA) - Bioenergetics 2007;1767(9):1073–101. http://dx.doi.org/10.1016/j.bbabio.2007.06.004.
[31] Fringeli UP, Günthard HH. Infrared membrane spectroscopy. Mol Biol Biochem Biophys 1981;31:270–332. http://dx.doi.org/10.1007/978-3-642-81537-9{_}6.
[32] Chen A, Liao S, Cheng M, Ma K, Wu L, Lai Y, et al. Spatiotemporal transcriptomic atlas of mouse organogenesis using DNA nanoball-patterned arrays. Cell 2022;185(10):1777–92. http://dx.doi.org/10.1016/j.cell.2022.04.003.
[33] Holman HY, Martin MC, Blakely EA, Bjornstad K, McKinney WR. IR spectroscopic characteristics of cell cycle and cell death probed by synchrotron radiation based Fourier transform IR spectromicroscopy. Biopolymers 2000;57(6):329–35. http://dx.doi.org/10.1002/1097-0282(2000)57:6<329::AID-BIP20>3.0.CO;2-2.
[34] Gupta S, Inman JL, Chant J, Obst-Huebl L, Nakamura K, M. CS, et al. A novel platform for evaluating dose rate effects on oxidative damage to peptides: toward a high-throughput method to characterize the mechanisms underlying the FLASH effect. Radiat Res 2023;200. http://dx.doi.org/10.1667/RADE-23-00131.1.
[35] Birarda G, Bedolla DE, Mitri E, Pacor S, Grenci G, Vaccari L. Apoptotic pathways of U937 leukemic monocytes investigated by infrared microspectroscopy and flow cytometry. Analyst 2014;139(12):3097–106. http://dx.doi.org/10.1039/c4an00317a.

[36] Martínez-Rovira I, Seksek O, Dokic I, Brons S, Abdollahi A, Yousef I. Study of the intracellular nanoparticle-based radiosensitization mechanisms in F98 glioma cells treated with charged particle therapy through synchrotron-based infrared microspectroscopy. Analyst 2020;145:2345–56. http://dx.doi.org/10.1039/C9AN02350J.

[37] Taillandier E, Liquier J. [16] Infrared spectroscopy of DNA. In: DNA structures part a: synthesis and physical analysis of DNA. Methods in enzymology, vol. 211, Academic Press; 1992, p. 307–35. http://dx.doi.org/10.1016/0076-6879(92)11018-E.

[38] Sofińska K, Wilkosz N, Szymoński M, Lipiec E. Molecular spectroscopic markers of DNA damage. Molecules 2020;25(3). http://dx.doi.org/10.3390/molecules25030561.

[39] Lipiec E, Birarda G, Kowalska J, Lekki J, Vaccari L, Wiecheć A, et al. A new approach to studying the effects of ionising radiation on single cells using FTIR synchrotron microspectroscopy. Radiat Phys Chem 2013;93:135–41. http://dx.doi.org/10.1016/j.radphyschem.2013.03.037.

[40] Gasparri F, Muzio M. Monitoring of apoptosis of HL60 cells by Fourier-transform infrared spectroscopy. Biochem J 2003;369(Pt 2):239–48. http://dx.doi.org/10.1042/BJ20021021.

[41] Barghouth PG, Melemenidis S, Montay-Gruel P, Ollivier J, Viswanathan V, Jorge PG, et al. FLASH-RT does not affect chromosome translocations and junction structures beyond that of CONV-RT dose-rates. Cold Spring Harbor Laboratory; 2023, http://dx.doi.org/10.1101/2023.03.27.534408, bioRxiv.

[42] Mantsch H, McElhaney R. Phospholipid phase transitions in model and biological membranes as studied by infrared spectroscopy. Chem Phys Lipids 1991;57(2):213–26. http://dx.doi.org/10.1016/0009-3084(91)90077-O.

[43] Derenne A, Claessens T, Conus C, Goormaghtigh E. Infrared spectroscopy of membrane lipids. In: Roberts GCK, editor. Encyclopedia of biophysics. Berlin, Heidelberg: Springer Berlin Heidelberg; 2013, p. 1074–81.

[44] Lewis RN, McElhaney RN. Membrane lipid phase transitions and phase organization studied by Fourier transform infrared spectroscopy. Biochim Biophys Acta (BBA) - Biomembranes 2013;1828(10):2347–58. http://dx.doi.org/10.1016/j.bbamem.2012.10.018.

[45] Sailer K, Viaggi S, Nüsse M. Kinetics of radiation- and cytochrome c-induced modifications in liposomes analysed by FT–Raman spectroscopy. Biochim Biophys Acta (BBA) - Biomembranes 1997;1329(2):259–68. http://dx.doi.org/10.1016/S0005-2736(97)00113-2.

[46] Ali MHM, Rakib F, Abdelalim EM, Limbeck A, Mall R, Ullah E, et al. Fourier-transform infrared imaging spectroscopy and laser ablation -ICPMS new vistas for biochemical analyses of ischemic stroke in rat brain. Front Neurosci 2018;12:647. http://dx.doi.org/10.3389/fnins.2018.00647.

[47] Halliwell B, Chirico S. Lipid peroxidation: its mechanism, measurement, and significance. Am J Clin Nutr 1993;57(5 Suppl):715S–24S; discussion 724S–725S. http://dx.doi.org/10.1093/ajcn/57.5.715S.

[48] Kinder R, Ziegler C, Wessels JM. Gamma-irradiation and UV-C light-induced lipid peroxidation: a Fourier transform-infrared absorption spectroscopic study. Int J Radiat Biol 1997;71(5):561–71. http://dx.doi.org/10.1080/095530097143897.

[49] Severcan F, Gorgulu G, Gorgulu ST, Guray T. Rapid monitoring of diabetes-induced lipid peroxidation by Fourier transform infrared spectroscopy: Evidence from rat liver microsomal membranes. Anal Biochem 2005;339(1):36–40. http://dx.doi.org/10.1016/j.ab.2005.01.011.

[50] Vileno B, Jeney S, Sienkiewicz A, Marcoux PR, Miller LM, Forró L. Evidence of lipid peroxidation and protein phosphorylation in cells upon oxidative stress photo-generated by fullerols. Biophys Chem 2010;152(1–3):164–9. http://dx.doi.org/10.1016/j.bpc.2010.09.004.

[51] Ruggeri FS, Marcott C, Dinarelli S, Longo G, Girasole M, Dietler G, et al. Identification of oxidative stress in red blood cells with nanoscale chemical resolution by infrared nanospectroscopy. Int J Mol Sci 2018;19(9). http://dx.doi.org/10.3390/ijms19092582.